Analysis of Microspherules from the Eldorado Bar

Wesley R. Brown

Abstract

Microspherule specimens collected from the Eldorado Bar located on the Missouri River in central Montana were submitted for further analysis. Use of heavy machinery and/or potential spherule producing tools directly at the collection site is rare, but additional anthropogenic sources require investigation. Microspherules have been reported as “abundant” at the collection site by regular visitors who use the Eldorado Bar as a dig site for sapphires and other minerals. However, no study has been conducted to determine the origin of these specimens. Some of the microspherules analyzed have trademark dendritic crystals that are indicative of quenching, often produced by impact processes. This analysis will utilize advanced spectroscopy methods to investigate the morphology and composition of the specimens in order to investigate the various processes that could’ve been involved in their formation.

Introduction

Microspherules can be generated through several processes, some of which are related to cosmic bodies. These can range from extraterrestrial impacts to airbursts, and even the atmospheric burn-up of small meteorites. These processes can produce extremely high temperatures exceeding 1800℃, leading to the melting and vaporization of most meteoritic material and much of the terrestrial material that is contacted. The resulting droplets may nucleate from the vapor phase or be dispersed as a fine mist resembling a more traditional ejecta in the liquid phase. Upon being projected high into the atmosphere, these droplets solidify and then deposit over vast areas. In the case of the Chicxulub impact, ejecta and microspherules are thought to cover ~5500 times the area of the source crater (Glass & Simonson, 2013). The widely dispersed microspherules are often found with a composition ranging from that of the impacted surface to pure meteoritic material. Microspherules formed through rapid quenching are typically glassy, and exhibit a 'dendritic' surface texture. In cases where there are high levels of PGEs, it is likely that there was a mixing with meteoric material, especially if it can be ruled out that the PGEs are derived from terrestrial surface features with known high levels (Sweatman, 2021).

There are also several terrestrial mechanisms that can produce microspherules. Volcanism is potentially the most common process. Silica-rich microspherules can be formed through the dispersal of hot magma during a volcanic explosion. This formation typically takes place at less than 1200℃. In addition, Iron-rich framboids, round quartz, and round hematite can be produced via erosional processes. However, these specimens lack surface quenching and thus present with no dendritic crystals, often making them easily discernible from cosmic related microspherules (Wu et al., 2013). There are many anthropogenic processes that can produce spherules as well. Many mechanical processes, smelting, certain power tools, and oxy-fuel cutting torches can produce iron spherules. In general, many iron spherules can be considered anthropogenic in origin unless nickel or platinum group elements are found (Larsen, 2017). Gross morphology can include dumbbell, teardrop, and cluster formations, although most are usually spherical. Specifically in impact spherules, it's not uncommon to discover spherules clustered with other materials, exhibiting a wide variation in size, 10um - 2mm (Glass & Simonson, 2013).

The objective of this study is to determine the potential origins of the microspherule specimens analyzed. Through the use of Scanning Electron Microscope (SEM), we investigate the overall surface and internal morphology. In addition, areas of interest are targeted for elemental composition analysis via Energy Dispersive X-ray (EDS). This allows for the identification of commonly found characteristics in various types of microspherules, providing a framework that can then be built upon. Once experimental procedures are concluded, the data is utilized to make plausible connections with the existing literature. Broad alignment with potential impact sources in the region are investigated. If locality, composition, and morphology are able to rule out anthropogenic production within the limitations found, then an impact related origin can be considered.

Methodology

Microspherule specimens are subdivided into magnetic and nonmagnetic groups. The magnetic group consisting of 4 microspherules were then set aside for analysis and deemed the focus of this study. The specimens were then individually cataloged by a randomly assigned number. Initial microscopic imaging is also conducted for cataloging purposes and filed in accordance with the specimen's number. Each spherule was placed under the SEM for initial analysis of

surface texture and composition and all recorded data was filed in the cataloged e-folders. The microspherules were then prepared for cross sectioning where each specimen was matched with a glass microscope slide that was numbered according to the catalog system. A target box was drawn onto each slide with a fine point sharpie in order to provide accurate margins for framing (fig 3, *A*). Masking tape was used for framing purposes in the order of 3 strips for each side, applied in a butt-end pattern (fig 3, *B*). The specimens were placed in the center of the frame, UV Loc-Tite was applied as an epoxy alternative, and the slides were left under UV for 10-12 hours for a complete cure (fig 3, *C; D; E*).

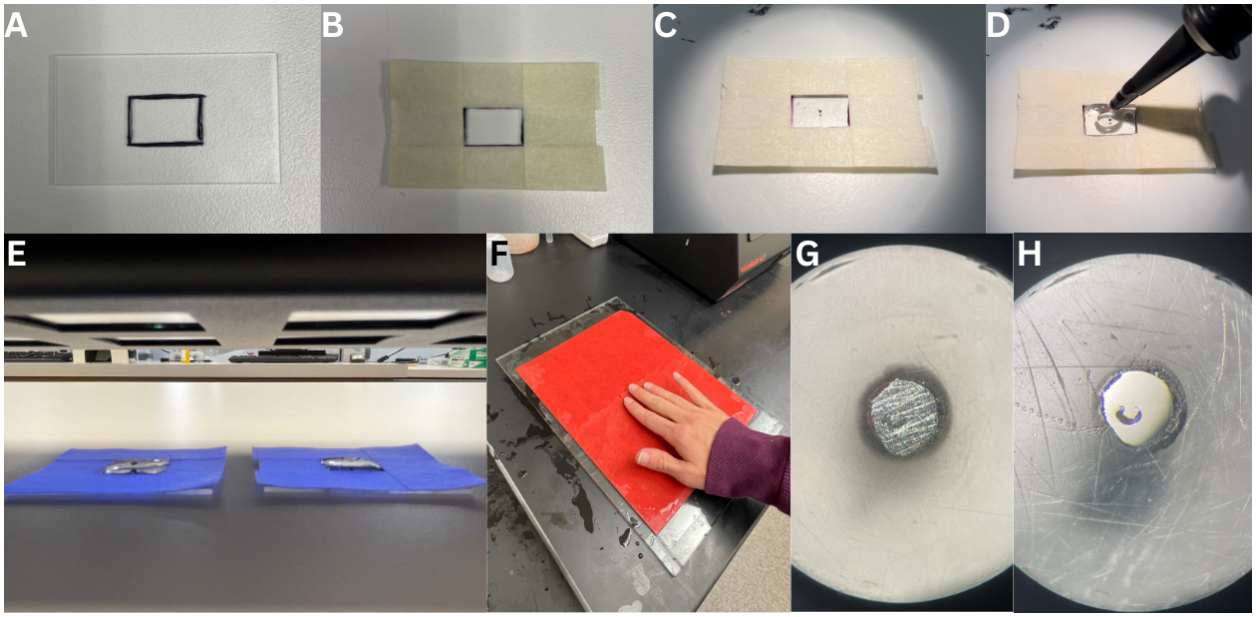

Fig 3. Framing margin outlined*(A)*. Framing application *(B)*. Spherule placement *(C)*. Epoxy/Loc-Tite application under stereomicroscope *(D)*. UV curing station *(E)*. Initial wet sanding at 450 grit *(F)*. Cross section at desired depth before higher grit progression *(G)*. Cross section after higher grit progression/polish *(H)*.

Wet sanding to obtain a cross section perspective was accomplished using a hand based technique with grit progression from 450g to 60,000g. A thin layer of tap water was applied to a 16 x 10in pane of glass as a method of stabilization for the sandpaper sheets. The specimens were then subjected to a timed sanding procedure (fig 3 *F*). Once desired depth was obtained via the lower grit sandpaper, progression to the highest grit was carried out accordingly until the specimen was polished (fig 3, *G; F*). Specimens 1 and 4 required an additional 1-2 minutes of each grit due to their larger size. Slides were then washed, dried and prepared for gold coating. Slides were placed in the sputter coater for ~15 minutes to ensure proper coverage. The slides

were then introduced into the SEM for cross section analysis of composition and morphology. Au and Pd were excluded from the EDS software prior to probing in order to properly account for the coating procedure and avoid false Au and Pd values during EDS analysis.

SEM images were taken of the whole cross section, points of nucleation or inclusions, and the crust-interior boundary sites. EDS targets focused on crystal formations, general interior and any inclusions or points of nucleation. A mostly holistic approach of broad exploration for predetermined key characteristics was taken. The EDS relative abundance values for three major areas of interest per spherule were used as data sets for mean value charts. This technique was deployed in order to provide a rough "whole specimen" composition. Standard deviation was included to ensure that variation in concentration was easily visible in the charts. The Mindat.com database was used as a point of reference to search documented minerals by chemistry.

Data & Observations

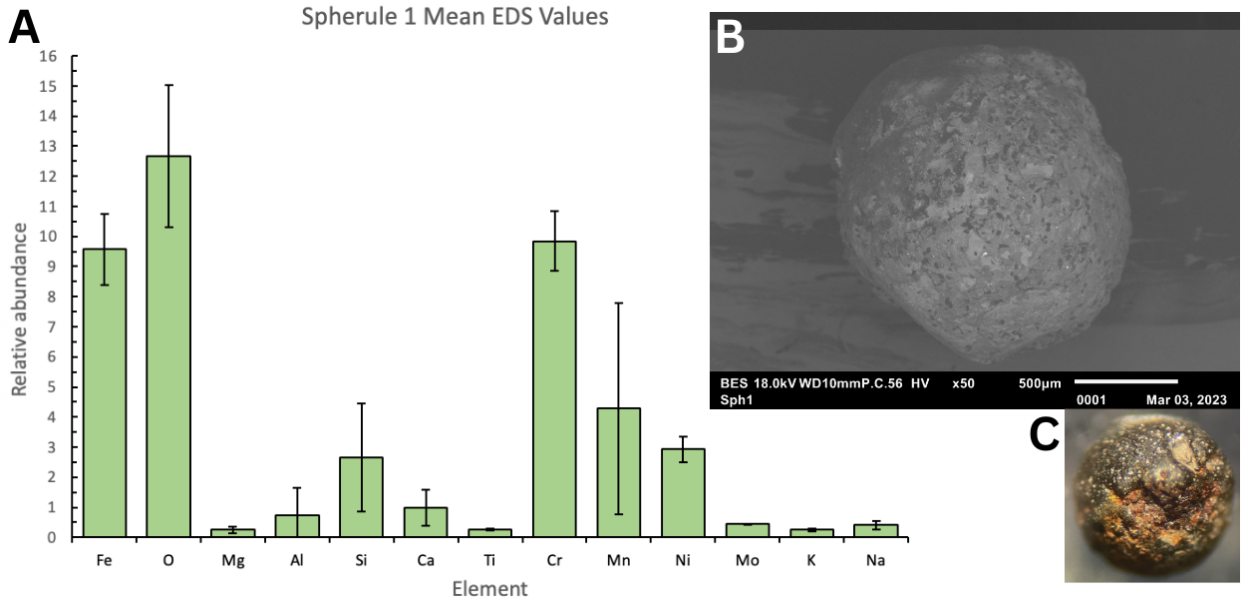

Element	Rel Abundance T1	Rel Abundance T2	Rel Abundance T3	Mean Values	SD (+/-)
Fe	9.78	10.64	8.28	9.56	1.24
O	15.32	11.86	10.83	12.67	2.4
Mg	.35	.25	.15	0.25	0.1

Al	.27	.19	1.77	0.74	0.89
Si	4.42	2.73	.84	2.66	1.79
Ca	.59	1.67	.68	0.98	0.59
Ti	.29	.23	.24	0.25	0.03
Cr	10.98	9.31	9.23	9.84	0.98
Mn	6.08	6.52	0.24	4.28	3.5
Ni	2.68	2.68	3.43	2.93	0.43
Mo	.45	.46	.42	0.44	0.02
K	.3	.21	.25	0.25	0.04
Na	.55	.27	.42	0.41	0.14

Fig 1. Mean element abundances and standard deviation derived from EDS targets on the spherule 1 surface *(A)*. Whole specimen image via SEM *(B)*. Whole specimen microscopic catalog image *(C)*. Graph *A* data set below.

Spherule 1 is about 1.3-1.5mm in diameter putting it on the upper end of spherules in terms of size. The SEM analysis of the surface revealed no evidence of dendritic crystals. It was mainly composed of iron oxides and small abundances of Si and Al which varied greatly with location. Due to the discontinuous nature of the Si and Al peaks, it seems likely that they're caused by terrestrial clay acquired while in a sedimentary environment. A low abundance of Mg was consistent along all areas of the surface.

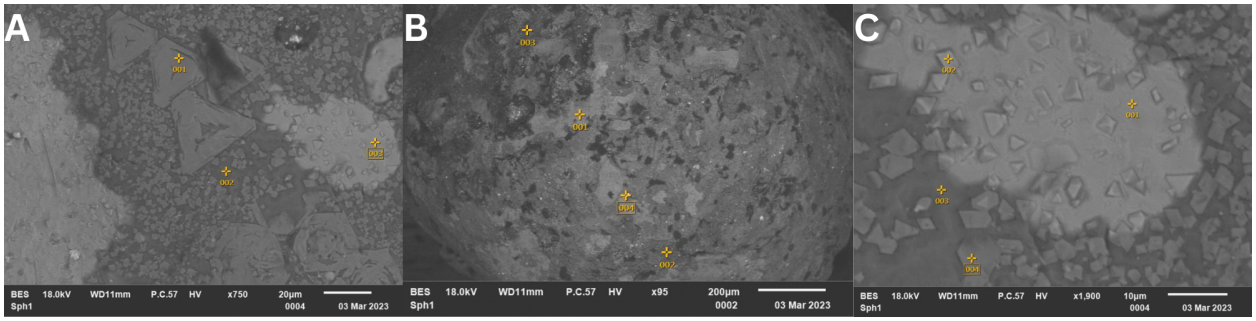

Fig 14. Skeletal triangular crystals in the central frame. Skeletal hexagonal crystals in bottom right of frame *(A)*. Wide angle capture of Spherule 1 surface *(B)*. Fe-Cr-Ni "pool" *(C)*.

Signs of supersaturation were present, with many skeletal hexagonal and triangular crystals observed (fig 14 *A*). EDS readings from the triangular crystals showed peaks of Cr followed by Mn and Fe in relative abundance. Based on composition alone, these crystals only produced one

match in the Mindat database known as hemleyite. A member of the ilmenite group, hemleyite was discovered in the shocked chondrite Suizhou L6 (Mindat, 2016). However interesting the observation may be, it doesn't necessarily serve as a form of direct evidence for an impact related origin. Light colored areas lacking specific shape or structure were observed and found to be composed of a Fe-Cr-Ni mineral that is also common in Spherules 3 and 4 (fig 14 *C*). These light colored mineral "pools" spotting the surface of the specimen are thought to be responsible for some of the speckles seen on the spherules mostly black surface in fig 1 *C*.

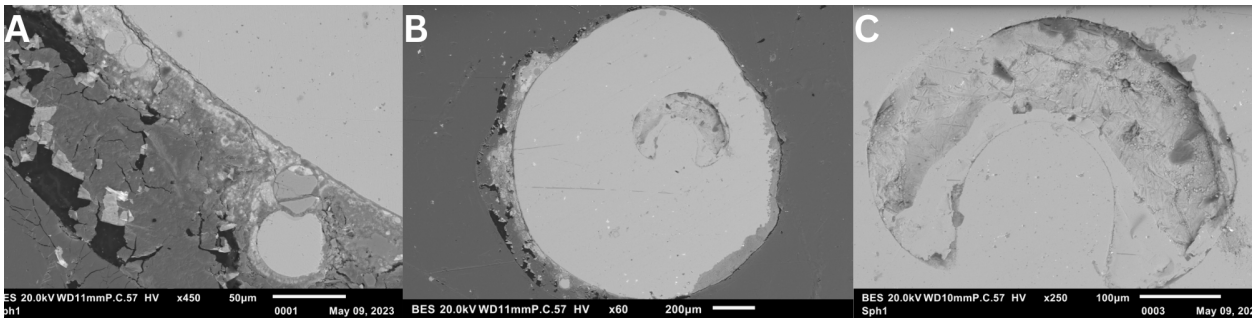

Fig 5. Spherule 1 Cross Section SEM Captures. Crustal boundary with Ni beads *(A)*. Whole specimen capture with lenticular cavity present *(B)*. Close up of the lenticular cavity *(C)*.

The cross section analysis of Spherule 1 revealed the interior is greatly dominated by iron oxides. Even the lenticular cavity (fig 5 *C*) is homogeneous in this respect. The only deviation from the iron oxides were small abundances of Ni which were localized to beads found within the crust (fig 5 *A*). In keeping with the morphological findings of the surface, no dendritic crystals were present in the cross section.

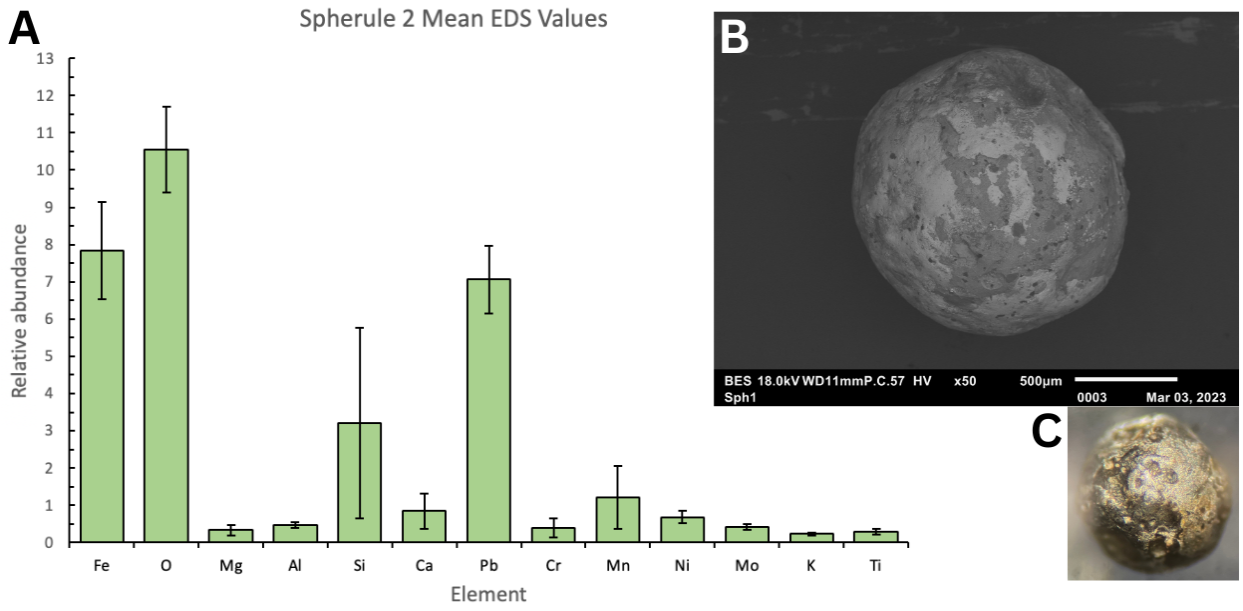

Element	Rel Abundance T1	Rel Abundance T2	Rel Abundance T3	Mean Values	SD (+/-)
Fe	6.34	8.52	8.66	7.83	1.29
O	11.86	9.69	10.1	10.55	1.15
Mg	.25	.26	.5	0.33	0.14
Al	.41	.44	.56	0.47	0.07
Si	2.73	5.97	.93	3.21	2.55
Ca	1.07	1.17	.3	0.84	0.47
Pb	8.1	6.43	6.66	7.06	0.90
Cr	.64	.38	.15	0.39	0.24
Mn	1.1	2.14	.42	1.20	0.84
Ni	.52	.68	3.43	0.68	0.16
Mo	.46	.47	.34	0.42	0.06
K	.2	.27	.22	0.23	0.03
Ti	.22	.29	.37	0.29	0.07

Fig 4. Mean element abundances and standard deviation derived from EDS targets on the spherule 2 surface *(A)*. Whole specimen image via SEM *(B)*. Whole specimen microscopic catalog image *(C)*. Graph *A* data set below.

Spherule 2 is about 1.2-1.5mm in diameter. It was considered to be of anthropogenic origin early on in the study. During the microscopic imaging for the experiment's catalog, it was noted that Spherule 2 presented features that are strikingly similar to anthropogenic I-type spherules (fig 15). In addition, a high abundance of lead was discovered throughout the spherules surface during EDS analysis and no dendritic crystals were observed. Due to these findings, no in depth analysis of the specimen was conducted.

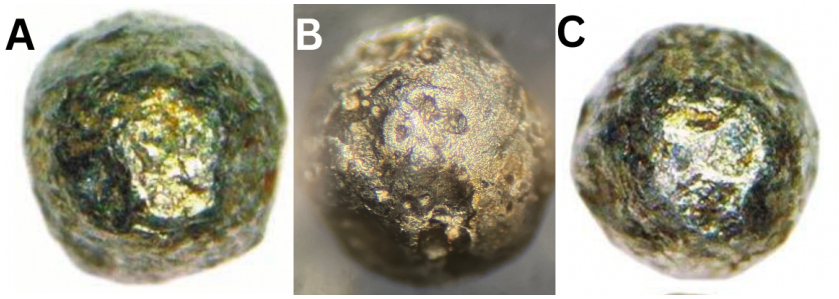

Fig 15. Anthropogenic I-type spherules, courtesy of Larsen, 2017 *(A, C)*. Spherule 2 microscopic catalog image *(B)*.

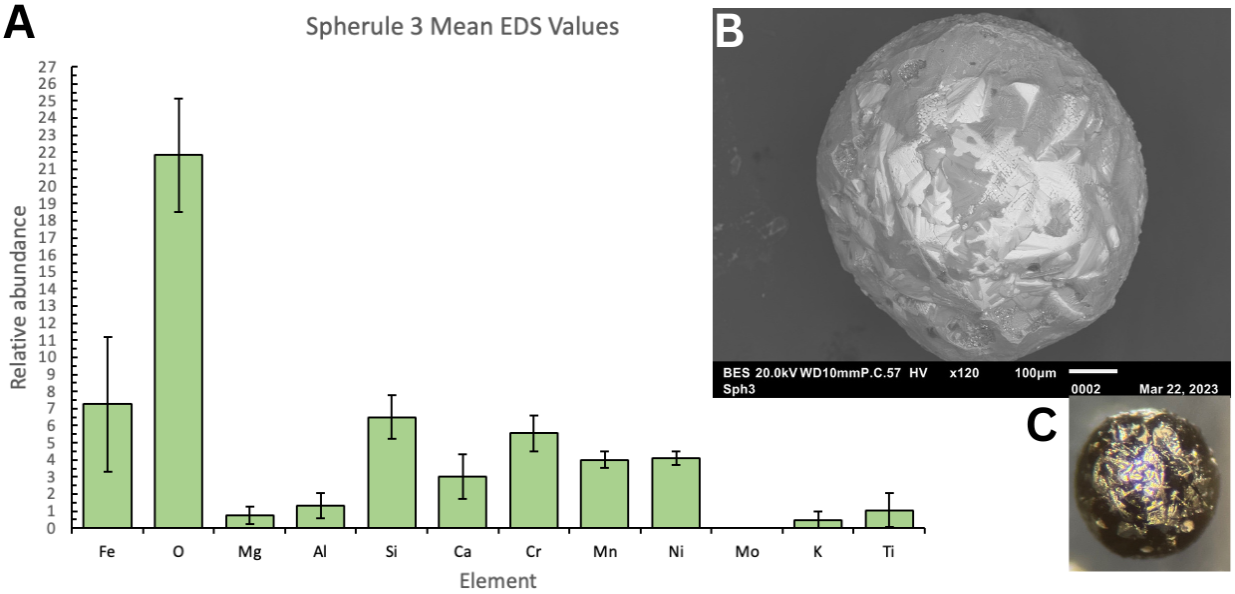

Element	Rel Abundance T1	Rel Abundance T2	Rel Abundance T3	Mean Values	SD (+/-)
Fe	11	3.16	7.64	7.26	3.93
O	25.59	19.26	20.68	21.8	3.21
Mg	1.01	1,07	0.17	0.75	0.50

Al	0.93	2.15	0.87	1.31	0.72
Si	7.96	5.97	5.56	6.49	1.28
Ca	3.68	1.51	3.85	3.03	1.32
Cr	6.62	4.58	5.44	5.54	1.02
Mn	4.26	4.28	3.43	3.99	0.48
Ni	-	4.4	3.8	4.1	0.42
Mo	-	-	-	-	-
K	-	0.84	0.13	0.48	0.50
Ti	-	1.76	0.37	1.06	0.98

Fig 6. Mean element abundances and standard deviation derived from EDS targets on the spherule 3 surface *(A)*. Whole specimen image via SEM *(B)*. Whole specimen microscopic catalog image *(C)*. Graph *A* data set below.

Spherule 3 is about 0.4-0.5 mm in diameter which is considerably smaller than both Spherule 1 and 2. The surface SEM analysis showed multiple large dendritic crystals which were targeted by EDS in two separate locations, both showing a composition of Fe, Ni and Cr (fig 7 *B*). There were no minerals in the Mindat database that could account for this composition. Low abundances of Al were found discontinuously along the spherules surface which could have been caused by a clay coating introduced through depositional processes after the spherules formation. The crust was composed of oxidized silicon or SiO_2 silicate that presented smaller but more consistent dendritic crystals throughout (fig 7 *A*).

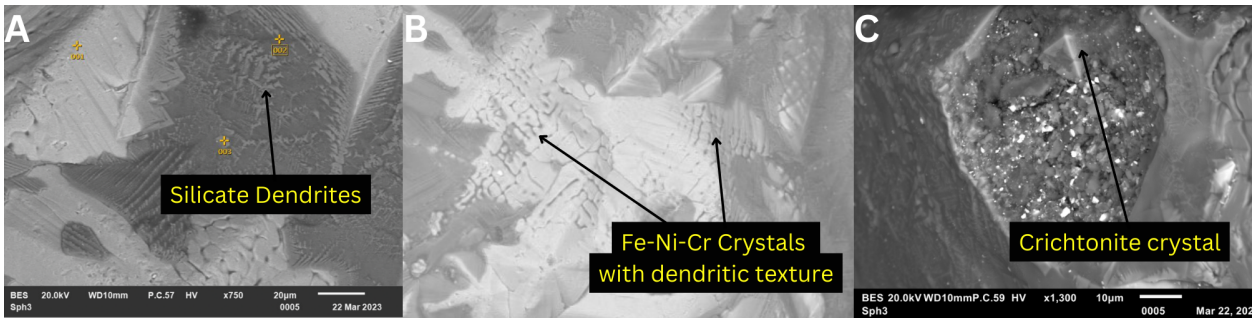

Fig 7. Dendritic silicate crystals prominent in the darker colored matrix of the crust *(A)*. Dendritic textures in the lighter colored Fe-Ni-Cr crystals *(B)*. Crichtonite crystal present in a keyhole formation produced by a missing Fe-Ni-Cr crystal *(C)*.

Non-dendritic crystals (complete crystal formations) were found in a keyhole left by one of the larger Fe-Ni-Cr crystals being dislodged (fig 7 *C*). Further examination using EDS and the Mindat database revealed them to be crichtonite crystals based on high abundances of Cr, Mn, and Ti followed by a low abundance of Fe. Based on the evidence of quenching processes and knowledge of material melting points, it's probable that the large Fe-Ni-Cr crystals began to cool and crystallize first at temperatures of ~1500℃-1800℃. The crichtonite crystals found deeper in the spherules crust were able to remain heated for an extended period while shielded by the Fe-Ni-Cr crystals above. This accounts for their overall complete structure and consequential lack of dendritic morphology even though they're likely to cool at higher temperatures such as those between 1650℃ and 1900℃. The remaining silicate crust cooled last and presumably underwent the most extensive quenching process evidenced by the innumerable dendritic silicate crystals present (fig 7 *A*).

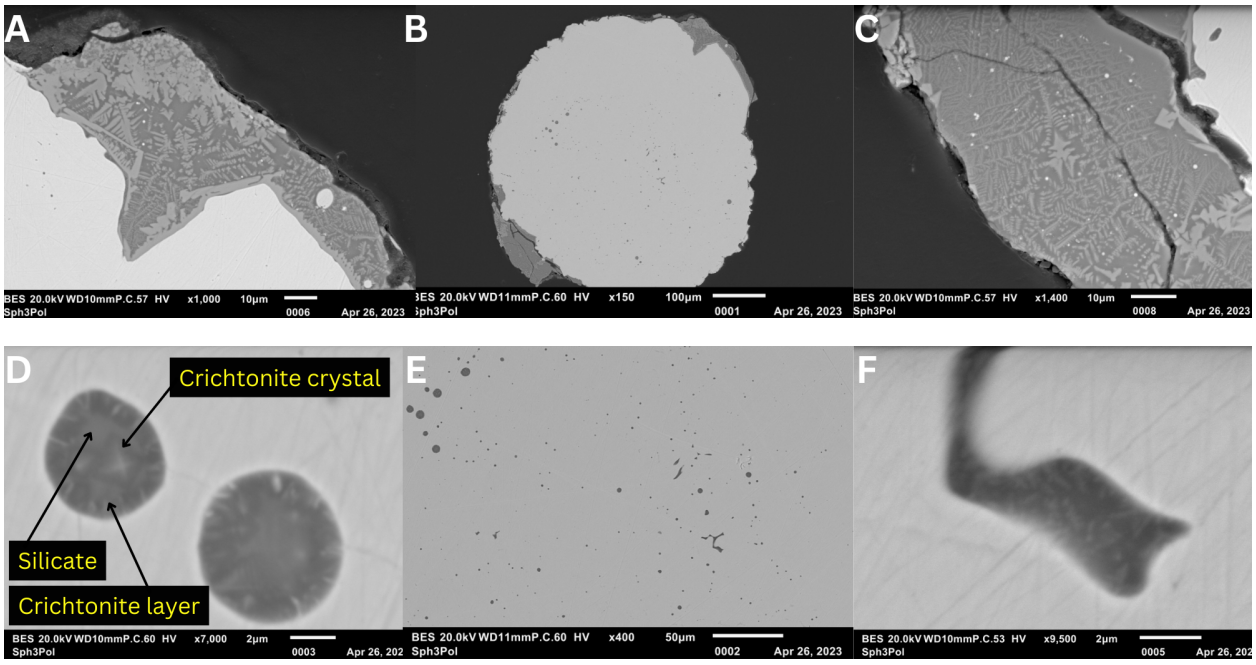

Fig 8. Dendritic silicate and Fe-Ni-Cr crystals spanning the entire crust thickness *(A & C)*. Whole specimen image via SEM *(B)*. Close up capture of two silicate inclusions within the Fe-Ni-Cr matrix featuring a Cr dominant outer layer and presumed crichtonite crystals in the central region *(D)*. Wide perspective capture of the Fe-Ni-Cr interior *(E)*. Close up capture of a silicate inclusion lacking the Cr dominant outer layer *(F)*.

The cross section analysis further supported the findings on the specimens surface. Dendritic Fe-Ni-Cr and silicate crystals can be seen in variation spanning the entire thickness of the crust (fig 8 *A* and *C*). The interior is composed of the same Fe-Ni-Cr that resulted in the larger surface

crystals. No dendritic crystals were observed within the greater interior such as those found on the surface and in the crust. However, silicate inclusions are present inside the interior which consist of a darker differentiated layer (fig 8 *D, E* and *F*). Dendritic and non-dendritic crystals are present within the inclusions (fig 8 *D*). The non-dendritic crystals closely resemble the crichtonite crystals observed in the keyhole. Due to resolution limitations, EDS target analysis was not possible, but a composition map roughly determined that the differentiated layer was composed of Cr and Fe. Although Ti was not included in the mapping, it's probable that this layer is equal in composition to the crichtonite crystals found in the crust.

All of this together concludes a silicate interior with crichtonite crystals, followed by a crichtonite outer differentiated layer. If a mix of molten silicate and crichtonite were trapped inside the spherule during formation and then underwent a partial differentiation process, this would explain the observations. Still, given the densities of the minerals involved, the silicate should have assumed the distal position of the inclusion. It's unknown how such a formation would occur, since the constituents were able to reach differentiation based on composition but not density.

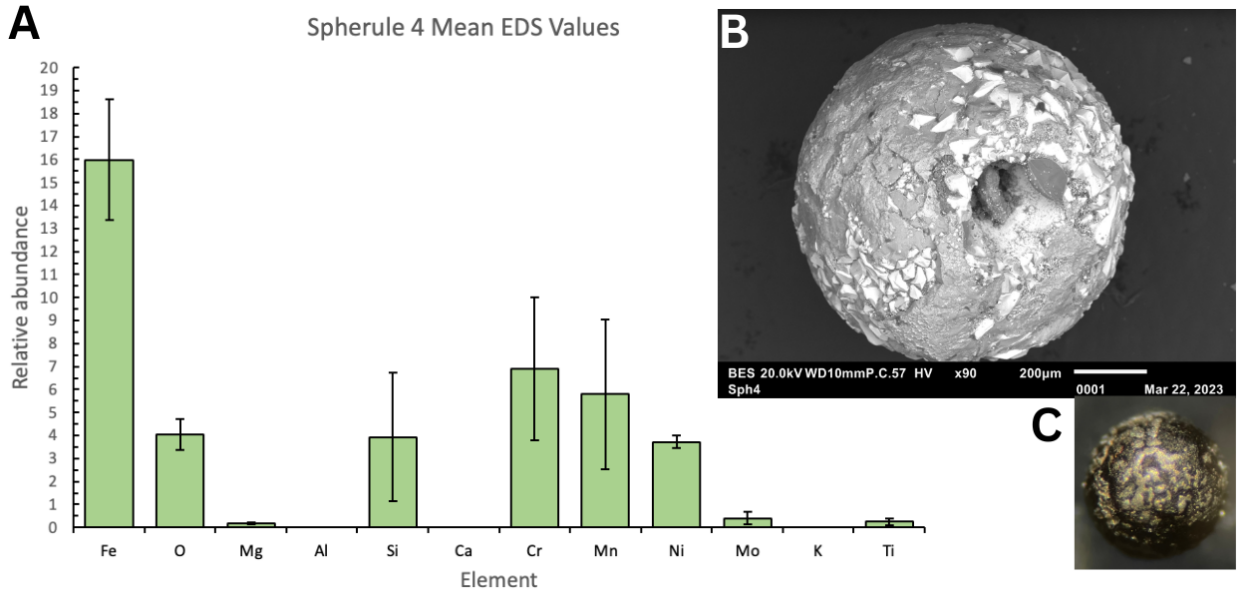

Element	Rel Abundance T1	Rel Abundance T2	Rel Abundance T3	Mean Values	SD (+/-)
Fe	18.8	15.2	13.8	15.9	2.61

O	3.38	4.73	3.99	4.03	0.67
Mg	0.21	0.16	0.14	0.17	0.03
Al	-	-	-	-	-
Si	1.16	6.73	3.9	3.93	2.78
Ca	-	-	-	-	-
Cr	4.93	5.29	10.48	6.91	3.1
Mn	4.64	9.46	3.29	5.79	3.24
Ni	3.97	3.41	3.81	3.73	0.28
Mo	0.68	0.13	0.42	0.41	0.27
K	-	-	-	-	-
Ti	0.11	0.26	0.37	0.24	0.13

Fig 9. Mean element abundances and standard deviation derived from EDS targets on the spherule 4 surface *(A)*. Whole specimen image via SEM *(B)*. Whole specimen microscopic catalog image *(C)*. Graph *A* data set below.

Spherule 4 is about 0.8-1mm in diameter. Many large crystals were observed and subsequently targeted for composition analysis via EDS. Three separate crystals were targeted and all contain the same Fe-Ni-Cr composition as found in Sherule 3. Little to no dendritic crystals were present on the specimens surface. A major difference between the Fe-Ni-Cr crystals in Spherule 3 and 4 is the lack of dendritic texturing at the lower portions in Spherule 4. This is in alignment with the oxygen abundance contrast found between Spherule 3 and 4. If Spherule 4 was exposed to a slightly less violent environment or even of equal extremes yet less overall exposure time, it may have resulted in more time for the crystals to fully form, avoiding further quenching and in turn, further oxidation. No crichtonite crystals were present which is reflected by the relatively low Ti abundance in the mean EDS values.

The surface crust is composed of silicate with low abundances of Mg throughout. One of the most prominent features in Spherule 4 is the central vesicle with a surface opening of ~180µm in width (fig 10 *B*). The vesicle proceeds to taper down to <50µm before reopening into a cavity of ~100µm in width at the center of the specimen (fig 11 *B*). The vesicle could have been formed by outgassing during the sperule's rapid cooling stage. It was later filled through depositional processes with what is presumed to be clay due to a high abundance of Si followed by Al and O.

Assuming the spherule was once molten, the Fe-Ni-Cr crystals cooled and crystallized first at temperatures of ~1500℃-1800℃ during formation. The remaining molten crust silicate cooled last and may have been influenced by late outgassing as evidenced by the 2 large silicate crystals located in and around the vesicles surface opening. An alternate explanation could place the silicate crystals there by the same processes that filled the vesicle.

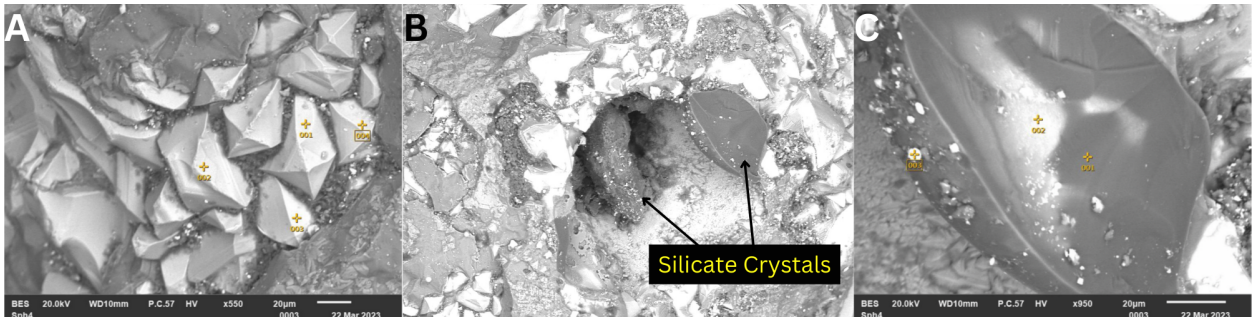

Fig 10. Completely formed Fe-Ni-Cr crystals present on the surface *(A)*. Two silicate crystals present in and around the vesicle surface opening *(B)*. Close up of the silicate crystal that's adjacent to the vesicle presenting fractured like morphology indicative of collision post crystallization.

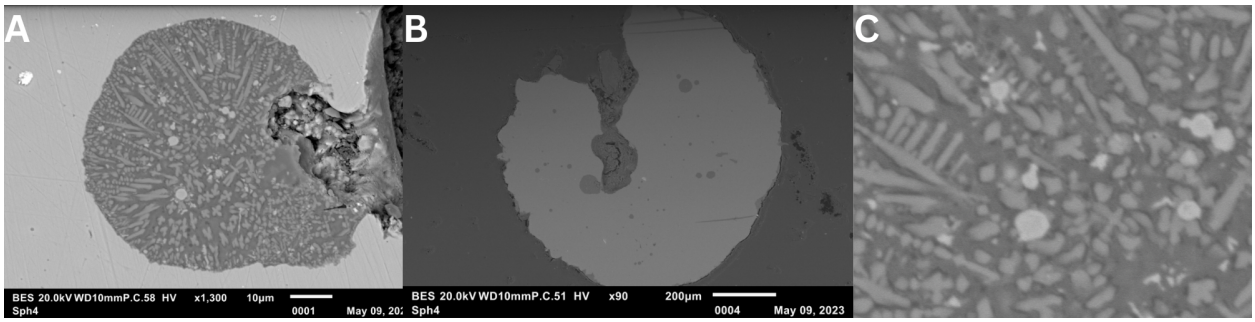

Fig 11. Largest of the present inclusions, composed of silicate with dendritic manganochromite and chromite beads *(A)*. Whole specimen cross section image via SEM *(B)*. Close up of inclusionary dendritic crystals forming the initial stages of christmas tree structures *(C)*.

The cross section analysis revealed an interior consisting of the same Fe-Ni-Cr composition found in Spherule 3. Approximately 20 inclusions with two of considerable size were also observed (fig 11 *A*). The inclusions consist of silicate with dendritic crystals composed of Cr, Mn and Fe in respective abundance. These peaks point to manganochromite as a potentially analogous mineral based on the Mindat database. The dendritic crystals are around 5µm in length on average with the longest being around 12µm. Partial tree-like dendritic formations with a central trunk such as those discussed in Galenko & Jou, 2019, were also observed as part of the

dendritic cluster (fig 11 *C*) . Ni peaks were not found within the dendritic crystals nor within the lighter colored beads that were composed almost entirely of chromite, as Fe and Cr were the only substantial peaks present.

Discussion

Limitations: A major limitation of the study would be the limited amount of specimens available. Many other studies within the literature conduct analysis across 100+ spherules. This limitation reduces the ability to better understand overall abundance of particular features and mineral composition amongst the spherules present in the area. Another limitation noted is the lack of information on the collection site. Besides the general area of the Eldorado Bar, it's not certain the exact location or depth at which the specimens were collected. This isn't of major concern for this specific study, however, if future studies look to build off this information in an attempt to determine more about the chronological deposition of spherules in the area then this information would be very useful. Lastly, while morphological analysis via SEM was within standard limits, the composition analysis via EDS presents certain limitations such as depth of information when compared to other methods like XRF (Singh et al., 2022).

Potential Origins: Yellowstone is ~270 km away from the collection site placing it well within the radius for microspherule disbursement. However, volcanism quickly becomes ruled out as a potential source for the spherules analyzed due to their general composition. Volcanism has never been found to produce iron rich spherules such as the specimens seen here. Instead, volcanic spherules are glassy and predominantly composed of silicate (Glass & Simonson, 2013).

Similar to the approach used with volcanism, when considering an extraterrestrial impact as the source, an emphasis on locality is put into place. The Beaverhead Impact Crater is ~254 km away from the collection site. The Beaverhead Impact occurred 600 million years ago and left a crater of ~60 km wide (Hargraves et al., 1990). This would have been well within the range necessary to disperse microspherules across modern day Montana including the Eldorado Bar. However, based on the USGS maps available for the region, the Eldorado Bar primarily sits on early holocene gravel and sediment. This would theoretically remove the Beaverhead Impact as a

potential source due to the age discrepancy. In fact, because of the stratigraphic age, only one potential impact seems a valid source candidate, the Younger Dryas Impact.

The Younger Dryas Impact has yet to be entirely confirmed, but over the last 15 years the evidence has been steadily growing. The impactor is thought to have been a comet or chondrite that underwent fragmentation upon entry, subsequently striking the Laurentide Ice Sheet in several places A black mat similar to the layer present at the K-Pg boundary has been found at sites across North America and Europe and thus deemed the Younger Dryas Boundary layer (YDB). The Younger Dryas occurred between 12,900-11,700 years before present, putting the Eldorado Bar sediment within the same time period. The Big Eddy collection site located in northwestern Montana was one of the first locations where impact spherules were discovered in sediment at the YDB (Firestone, 2007).

Fig 12. Google Earth capture with the Eldorado Bar marked by the purple pin. The Beaverhead Impact Crater and the Big Eddy site are marked by yellow pins.

If the spherules analyzed in this study are the product of any extraterrestrial impact, then the Younger Dryas Impact is the most probable by age and location of proxy evidence. The impact spherules studied at the YDB do share similarities with the specimens analyzed in this study such as being iron rich and having dendritic crystals present. However, it's noted that only a handful of impact spherules discovered at the YDB were greater than 1mm making it rather unlikely that Spherule 1 could be considered related. In addition, none of the YDB spherules have protruding crystals present on the surface such as the spherules analyzed here. Instead, they're mostly smooth and homogenous on the surface with dendritic crystals throughout. Lastly, not a single spherule from the YDB has been reported with large abundances of chromium/chromium (Wu et al., 2013; Firestone, 2007).

Further investigation of chromium/chromium oxide abundance in extraterrestrial impact research led to Mn/Cr ratio studies in chondrites. This became of interest due to the consistent and mostly bewildering Mn and Cr peaks found amongst the spherules. Manganese-chromium systematics are well documented throughout the literature and a direct relationship between Mn and Cr has been found in H and L type chondrites (Nichiporuk et al., 1967). Average ratios of Mn/Cr were studied in several publications that utilized X-ray fluorescence (XRF) on chondrite samples reporting .57 $\pm$ 0.02 for H type chondrites and .63 $\pm$ 0.03 for L type chondrites reported in Yates et al., 1968.

Source	Mn/Cr	SD (+/-)
Sperule 1	0.43	0.2
Spherule 3	0.72	0.07
Spherule 4	0.83	0.31
Yates et al., 1968 (L type)	0.57	0.02
Yates et al., 1968 (H type)	0.63	0.03
Nichiporuk et al., 1967	0.52	0.08
Nyquist et al., 2001 (Sample C)	0.68	0.31
Nyquist et al., 2001 (Sample B)	0.81	0.3

Fig 2. Mn/Cr ratios and standard deviation of Spherule 1, 2 and 3 compared to those reported in Yates et al., 1968; Nichiporuk et al., 1967; Nyquist et al., 2001.

This is supported by a more recent study published in Meteoritics and Planetary Science where around 40 chondrite samples from two separate chondrites were found to have Mn/Cr ratios of .68 and .81 with standard deviation values of .31 and .30 respectively (Nyquist et al., 1998). Fig 2 represents those ratios alongside the Mn/Cr ratio calculated from the mean EDS values of the specimens analyzed here. Discrepancy in the depth of information between XRF and EDS may account for the larger SD in the spherules from this analysis. If mixing with chondritic material were to be considered as a potential source for the spherules, the overall abundance of Cr and Mn remain problematic. The studies shown in fig 2 report ~0.3% Cr and ~0.2% Mn in abundance of the chondrite samples, which is within the typical range for chondrite abundances in all of the available literature. This would put the abundances found in the spherules far beyond what has been reported historically in the chondrite samples and thus making it nearly impossible that they derived from a similar body.

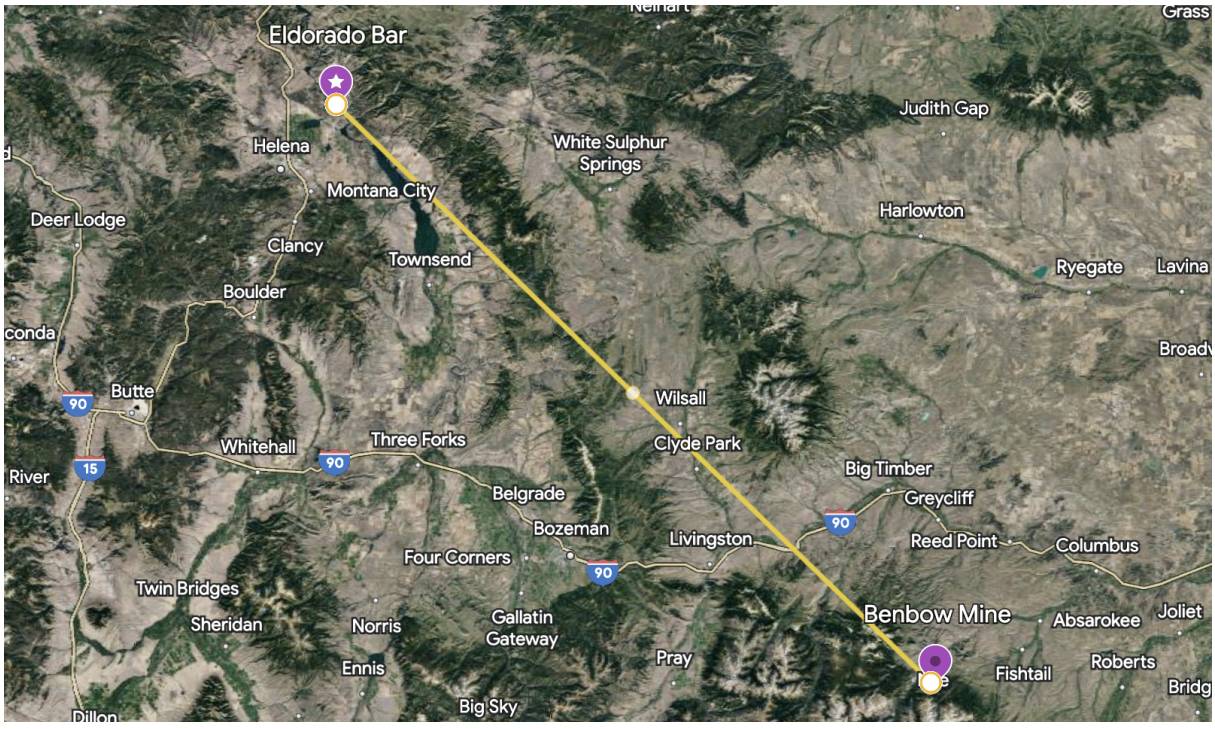

Fig 13. Google Earth capture representing the location and distance between the Eldorado Bar and the Benbow Chromite Mine (~217 km).

Chromium and chromium oxides are often used/produced in industrial applications for stainless steel coating, electroplating, and extraction of chromium from chromite ore (Hu et al., 2021). A deeper investigation of the state of Montana's industrial facilities with the help of the Montana

Bureau of Mines and Geology revealed the presence of the Benbow Chromite Mine ~217 km southeast of the collection site (fig 13). The mineral extraction processes taking place at Benbow Mine such as chromite ore being crushed and roasted in the presence of free air, are more than capable of producing the spherules analyzed in this study. The most probable means of transportation would be through the use of mining equipment at the Eldorado Bar that had previously been exposed to the Benbow Mine environment. In addition, strong winds could carry the spherules across large distances.

Conclusion

Within the limitations stated, the findings from microspherules analyzed were not able to rule out anthropogenic means. Potential impact and volcanic related origins were thoroughly investigated and exhausted and consistently failed to align with the analysis, leading to a conclusion of anthropogenic sources with high confidence. Based on the findings in this study, the remaining non magnetic spherules should undergo analysis to determine if any characteristics are consistent with those found in these specimens. This would provide insights for future research on locally related spherules. Future research should focus on studying the microspherules in the area through the lens of potential environmental pollutants. Deeper study of the stratigraphy at the collection site and the depth of spherule dispersion could be a useful next step towards research on long-term environmental implications.

A secondary discovery that emerged from this study is a point of miscommunication happening in the discourse surrounding the use of dendritic crystals as markers for impact spherules. While several publications outright state that the presence of dendritic crystals alone is a marker for impact related origins (Sweatman, 2021; Wu et al., 2013; LeCompte et al., 2012; Firestone, 2007), this is simply a misrepresentation of the evidence. Instead, dendritic crystals within specific limitations can be used as quality markers for impact origins and those limitations should be clearly outlined.

Citations

Galenko, P. K., & Jou, D. (2019). Rapid solidification as non-ergodic phenomenon. *Physics Reports*, *818*, 1–70. https://doi.org/10.1016/j.physrep.2019.06.002

Glass, B. P., & Simonson, B. M. (2013). *Distal impact ejecta layers: A record of large impacts in sedimentary deposits*. Springer Berlin Heidelberg.

Hargraves, R. B., Cullicott, C. E., Deffeyes, K. S., Hougen, S., Christiansen, P. P., & Fiske, P. S. (1990). Shatter cones and shocked rocks in southwestern Montana: The Beaverhead Impact Structure. *Geology*, *18*(9), 832. https://doi.org/10.1130/0091-7613(1990)018<0832:scasri>2.3.co;2

Hu, S., Wang, D., Li, X., Zhao, W., Qu, T., & Wang, Y. (2021). Enrichment characteristics of CR in chromium slag after pre-reduction and melting/magnetic separation treatment. *Materials*, *14*(17), 4937. https://doi.org/10.3390/ma14174937

Larsen, J. (2017). *In Search of Stardust: Amazing Micrometeorites and their terrestrial imposters*. Voyageur Press, an imprint of The Quarto Publishing Group.

LeCompte, M. A., Goodyear, A. C., Demitroff, M. N., Batchelor, D., Vogel, E. K., Mooney, C., Rock, B. N., & Seidel, A. W. (2012). Independent Evaluation of conflicting microspherule results from different investigations of the younger Dryas impact hypothesis. *Proceedings of the National Academy of Sciences*, *109*(44). https://doi.org/10.1073/pnas.1208603109

Nyquist, L., Lindstrom, D., Mittlefehldt, D., hih, C.-Y., Wiesmann, H., Wentworth, S., & Martinez, R. (2001). Manganese-chromium formation intervals for chondrules from the Bishunpur and Chainpur meteorites. *Meteoritics & Planetary Science*, *36*(7), 911–938. https://doi.org/10.1111/j.1945-5100.2001.tb01930.x

Singh, V. K., Kawai, J., & Tripathi, D. K. (2022). *X-Ray Fluorescence in Biological Sciences: Principles, instrumentation, and applications*. John Wiley & Sons, Incorporated.

Sweatman, M. B. (2021). The younger Dryas impact hypothesis: Review of the impact evidence. *Earth-Science Reviews*, *218*, 103677. https://doi.org/10.1016/j.earscirev.2021.103677

Wu, Y., Sharma, M., LeCompte, M. A., Demitroff, M. N., & Landis, J. D. (2013). Origin and provenance of spherules and magnetic grains at the younger dryas boundary. *Proceedings of the National Academy of Sciences*, *110*(38). https://doi.org/10.1073/pnas.1304059110

Yates, A. M., Tackett, S. L., & Moore, C. B. (1968). Chromium and manganese in chondrites. *Chemical Geology*, *3*(4), 313–322. https://doi.org/10.1016/0009-2541(68)90036-3